Article:

Lister, S., Baxter, G.J. and Jackson, M. (2025) Titanium-S23: A new alloy with ultra-high tensile toughness directly from the solid-state processing of recycled Ti–6Al–4V and Ti–5Al–5Mo–5V–3Cr powders using field assisted sintering technology. Advanced Engineering Materials, 27 (17). 2500572. ISSN: 1438-1656

https://doi.org/10.1002/adem.202500572

ADVANCED ENGINEERING MATERIALS
www.aem-journal.com

Titanium-S23: A New Alloy with Ultra-High Tensile Toughness Directly from the Solid-State Processing of Recycled Ti–6Al–4V and Ti–5Al–5Mo–5V–3Cr Powders using Field Assisted Sintering Technology

Samuel Lister, Gavin J. Baxter, and Martin Jackson*

This article exploits field-assisted sintering technology (FAST) as a sustainable solid-state processing route for alloy design, to produce a novel β-rich, $\alpha + \beta$ titanium alloy, Ti–5.5Al–4.5V–2.5 Mo–1.5Cr, with exceptional tensile toughness properties. Surplus Ti–6Al–4V and Ti–5Al–5Mo–5V–3Cr powders, in size fractions that are outside the nominal particle size distribution range of additive manufacturing processes, are mixed and sintered with a range of FAST processing parameters. Microstructural analysis and Vickers hardness measurements optimize the processing parameters (to a maximum of 395 HV). Large-scale billets (250 mm diameter) are subsequently produced, allowing the extraction of tensile, Charpy, and microstructural analyses samples. Tensile testing reveals that this new synergistic alloy has an exceptional balance of strength–ductility (UTS = 1110 MPa, Elongation > 15%), that is, tensile toughness, in the as-FAST condition—exceeding the properties of the parent alloys. Microstructural analysis reveals the presence of fine-scale alpha precipitates to which the superior mechanical properties can be attributed. This study provides the basis for future investigations focused on this novel alloy, termed S23 by Rolls Royce plc, which can be produced from commercial surplus powder and scrap streams.

1. Introduction

Titanium alloys are widely utilized in fan and compressor applications in the “cold” or front end of aeroengines due to their excellent strength-to-weight ratio. Designers constantly seek to further reduce weight and increase the creep and fatigue lives of aeroengines, to reduce fuel consumption and improve efficiency. A range of properties are important for different titanium aeroengine components, including impact resistance, fatigue life, damage tolerance, fracture toughness, creep strength, and ductility. One method to achieve enhanced properties is through the development of new alloys. This article will detail initial work on a new alloy, serendipitously discovered through the utilization of commercially available powder outside the nominal size range for additive manufacturing (AM) processes. The results illustrate that this alloy has improved properties compared to both parent alloys.

Over recent years, the increase in popularity of 3D printing or powder AM has led to an increase in the commercial availability of prealloyed powders and wire. Large amounts of the powder atomized for such processes are unusable due to not being within strict particle size distribution (PSD) limits and are often stockpiled or remelted to be reatomized, wasting energy and high-quality material. In addition, vast amounts of waste machining swarf are generated during the manufacture of titanium aerocomponents. The surplus powder has provided opportunities to combine and join existing alloys in ways not previously explored to create titanium–titanium composites. Pope et al.[1] exploited the field-assisted sintering technology (FAST) process, also known as spark plasma sintering (SPS), to diffusion bond (DB) two or more titanium alloys in a process referred to as FAST-DB. FAST can effectively consolidate almost any powder size or morphology (including machining swarf[2]). The FAST-DB method has also been demonstrated on nickel-based superalloys for aerospace applications.[3] In the work of Pope et al.[1] a region of enhanced microhardness was discovered with fine-scale α-precipitates in the bond region between Ti–6Al–4V (Ti–64) and Ti–5Al–5Mo–5V–3 Cr (Ti-5553), as shown in **Figure 1**. Other alloy combinations trialed did not exhibit such behavior, but showed a smooth transition in microhardness from one alloy to the other. Typically, such fine microstructures are achieved through significant thermomechanical processing routes, not the relatively slow cooling inherent during large-scale FAST processing (250 mm diameter). Tensile tests of samples containing such a DB failed in the lower-strength alloy, implying

---

S. Lister, G. J. Baxter, M. Jackson
School of Chemical
Materials and Biological Engineering
University of Sheffield
Sir Robert Hadfield Building, Mappin Street, Sheffield S1 3JD, UK
E-mail: sam.lister@sheffield.ac.uk

The ORCID identification number(s) for the author(s) of this article can be found under https://doi.org/10.1002/adem.202500572.

DOI: 10.1002/adem.202500572

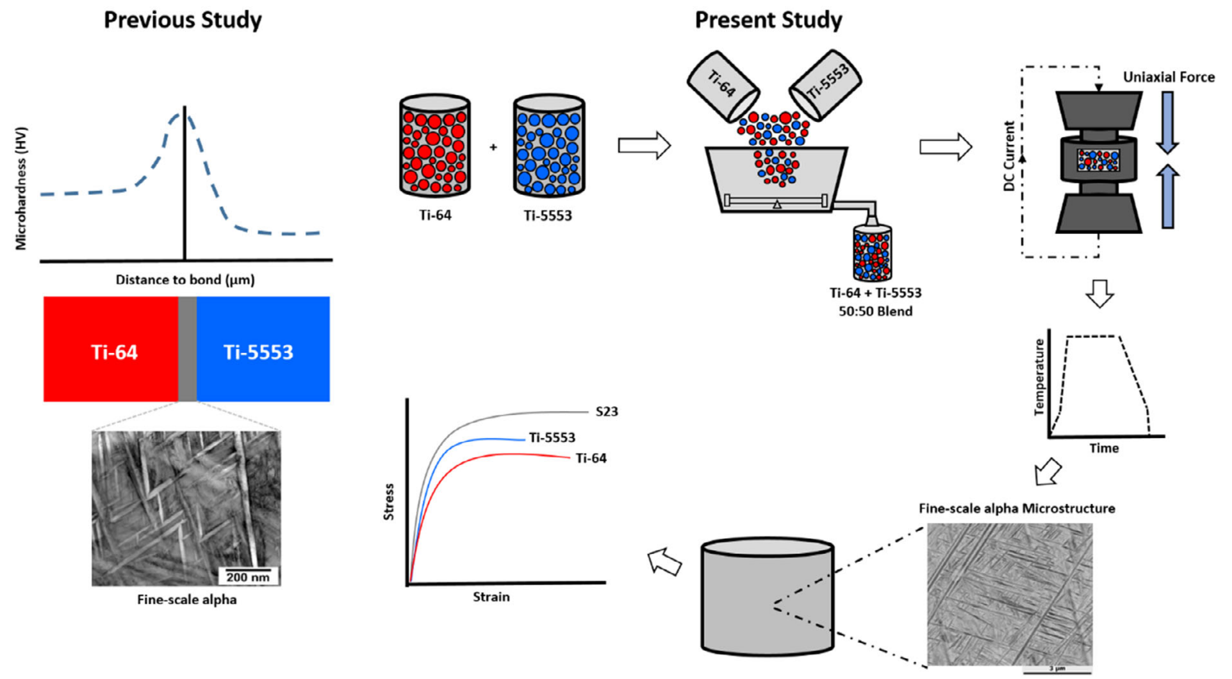

Figure 1. Schematic demonstrating the motivation for the mixing of the two powders (left) and the approach taken in this study (right), building on the previous work by Pope et al. The left SEM image of this figure is reprinted with permission.[1] Copyright 2019, Elsevier.

a high-strength bond region. Davis et al.[4] experimented with wire-arc additive manufacture to produce dual-alloy microstructure components, alternating layers of Ti-64 and CP-Ti wire feedstock. Termed an "alloy–alloy" composite, they proposed potential fracture toughness benefits due to the increased crack path disruption from the dual microstructures. Kennedy et al.[5] expanded this approach to Ti-64 and Ti-5553 alloys, the same alloys under investigation in this article. The chemical gradient between the two alloys was characterized in detail; however, no microhardness data across the bond region was presented and this would make an interesting comparison with the results published by Pope et al.[1] Similarly, Zafari and Xia[6] developed a concept termed HYbrid Ti Alloy (HYTA), utilizing selective laser melting to combine Ti-64 and Ti-5553, to achieve a combination of microstructures not achievable in single-alloy systems. This was developed further, into a ternary HYTA, with the addition of CP-Ti[7] and achieved a good balance of strength–ductility, attributed to the coincidental activation of several deformation modes, allowing the deformation to transfer between various regions of the structure. While other researchers have combined or joined Ti-64 and Ti-5553 by various methods, none have reported the same region of enhanced microhardness and corresponding fine-scale α microstructure as Pope et al.[1] discovered through FAST processing.

The high strength in the DB region between Ti-64 and Ti-5553 was attributed to the presence of very fine-scale α laths, confirmed by transmission electron microscopy (TEM) observation. Many researchers have attempted to engineer fine-scale α microstructures through various methods. Mantri et al.[8] compared the mechanical properties of Ti alloy β-21S with fine or coarse α precipitates. The different-sized precipitates were produced via different heat treatments. Fine-scale α produced an increase of around 250 MPa in strength and around 8% elongation to failure, demonstrating the balance of strength–ductility achievable. Devaraj et al.[9] applied press-and-sinter and heat treatment routes to a Ti–1Al–8V–5Fe (Ti-185) alloy in TiH_2 form to produce a hierarchical fine-scale α nanostructure, with very high tensile strengths of up to 1690 MPa. Zheng et al.[10] investigated the role of ω phase on the precipitation of extremely refined intragranular α in Ti-5553, observing that the ω phase significantly influenced the precipitation via compositional and stress fluctuations that were caused by nonuniformities in the β-matrix and acted as the preferred nucleation sites for the α-phase. ω-assisted α precipitation in Ti-5553 has also been investigated by Coakley et al.[11] A recent study by Jia et al.[12] investigated the role of the ω phase on heterogeneous α precipitation in $\alpha + \beta$ alloys, despite this mechanism previously being thought of as exclusively present in the metastable β-alloys. One study by Wang et al.[13] demonstrated the possibility of producing a fine-scale α microstructure through slow cooling, by producing an alloy of composition Ti–15.5V–3.6Al–1.8Fe, with elevated hardness of 474 HV reported for as-cast, coarse-grained buttons of alloys close to this composition. A number of other formation mechanisms have been discovered to be responsible for the precipitation of fine-scale α such as phase separation of the β-phase[14] and a pseudospinodal mechanism.[15] No studies have been published in the literature on combining and solid-state (FAST) processing Ti-64 and Ti-5553 alloy powders to produce a fine-scale α microstructure via slow cooling. This article addresses this gap in the literature and presents initial findings of the synergy created by combining the two commercial aerospace alloys to produce a new alloy composition, Ti–5.5Al–4.5V–2.5Mo–1.5Cr.

2. Experimental Section

The PSD of the powders used in this study was measured using a Malvern Mastersizer 3000 using the wet dispersion method. Ten measurements were made for each powder sample and the results were averaged to give the Dx(10), Dx(50), Dx(90), and relative span values shown in **Table 1**. Relative span allows the span of the distributions to be compared and was calculated using Equation (1)

$$\text{Relative Span} = \frac{\mathrm{D}x(90) - \mathrm{D}x(10)}{\mathrm{D}x(50)} \tag{1}$$

Gas-atomized (GA) Ti-5553 powder (TLS Technik Spezialpulver) was utilized for all small-scale samples and advanced plasma atomized (APA) Ti-5553 (AP&C) powder was used for both large-scale samples, Ti-64 plasma rotating electrode-processed (PREP) (Timet) powder was used for both small and large-scale samples. Secondary-electron (SE) micrographs of each powder are shown in **Figure 2**.

Two samples of the new alloy produced using FAST (Billet 1 and Billet 2) were chemically analyzed by Intertek, alongside a powder sample of both Ti-64 (PREP) and Ti-5553 (APA). The quantity of Ti, Al, V, Mo, Cr, and Fe was measured via inductively coupled plasma–optical emission spectroscopy, the quantity of C and S was measured via combustion analysis, and the quantity of N, O, and H was measured via inert gas fusion. The results are summarized in **Table 2**.

Except where explicitly stated, all samples were produced with a mix ratio of 50% Ti-64% and 50% Ti-5553, by volume, due to the slight differences in density of the two powders. This approach was taken to allow the maximum number of interfaces between the particles of the two powders, promoting diffusion and subsequent homogenization. Mixing was performed manually for 10 min by filling a large powder drum and rotating around 3 axes.

Table 1. The measured PSD of each powder used in this study.

	Dx(10) [μm]	Dx(50) [μm]	Dx(90) [μm]	Relative Span
Ti-5553 GA	18.8	58.2	157	2.37
Ti-64 PREP	60.9	82.3	111	0.61
Ti-5553 APA	40.3	55.5	81.3	0.74

Small-scale FAST samples were produced using a FCT Systeme GmbH HP D 25 SPS furnace located in the Royce Discovery Centre (RDC) at the University of Sheffield. 18 g of mixed Ti-64 and Ti-5553 powder was sintered at a range of processing temperatures from 975 to 1200 °C, for a range of processing times from 10 to 60 min. All samples were produced using a 20 mm-diameter graphite die. Following sintering the current was switched off and the sample was allowed to cool freely in the vacuum chamber.

Large-scale FAST billets, 1 and 2, were produced using a FCT Systeme GmbH HP D 250/C SPS furnace located at the same facility. 5.3 kg of mixed Ti-64 and Ti-5553 powder was sintered at 1200 °C for 60 min. Billet 1 was produced using a 200 mm diameter graphite die and the "rapid cooling" function of the sintering furnace. Billet 2 was produced using a 250 mm diameter graphite die in the standard sintering setup. A maximum uniaxial pressure of 35 MPa and pulsed current time of 15 ms on, 5 ms off, was maintained for all FAST samples.

Small-scale samples were sectioned parallel to the compression direction and prepared metallographically using SiC grit grinding papers followed by polishing with 0.06 μm colloidal silica mixed with 30% hydrogen peroxide in a ratio of 9:1. Full-size round tensile bars (ASTM E8 specimen 1) were extracted from Billet 1 and 2 via wire-EDM and machined to size. Standard sized Charpy V-notch test specimens were extracted from Billet 2 via wire EDM. Microstructural analysis samples were sectioned from the large-scale billets in various locations before the same metallographic routine was applied. TEM samples were prepared from the bulk material via the thin foil method. Samples were first sectioned to ≈0.7 mm thickness using a Secotom-50, before being mechanically ground by hand to ≈100 μm thick. 3 mm diameter circles were then extracted and electropolished using

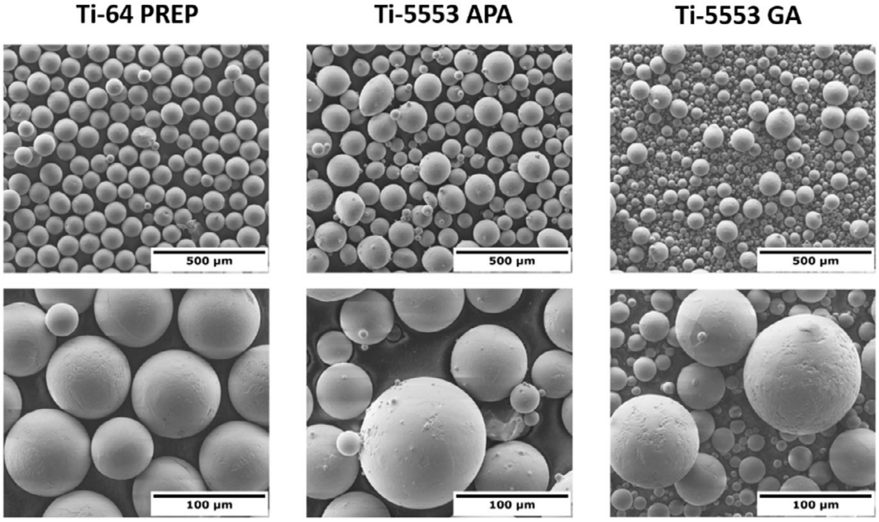

Figure 2. SE micrographs of the three powders used in this study.

Table 2. The measured composition of each major and minor element for billets 1 and 2 and samples of the initial powder for each alloy. All given in wt% except for N, O, and H given in ppm.

	Ti	Al	V	Mo	Cr	Fe	C	S	N	O	H
Billet 1	85.34	5.75	4.52	2.52	1.47	0.19	0.024	0.001	260	1423	47
Billet 2	85.60	5.61	4.43	2.51	1.43	0.19	0.028	0.002	187	1536	39
Ti-64 powder	89.46	6.22	3.95	<0.01	<0.01	0.10	0.034	0.001	283	2065	33
Ti-5553 powder	81.68	5.12	4.96	4.94	2.857	0.27	0.013	0.002	133	923	22

a Struers Tenupol-5 twin-jet electropolisher with a solution of 60% methanol, 37% 2-butaxyethanol, and 3% perchloric acid at −35 °C, with voltage 28 V and flow rate of 16.

Cross-polarized light microscopy was conducted using a Nikon optical light microscope with Buehler Omnimet 9.5 software. Scanning electron microscopy (SEM) was performed using a FEI Inspect F50 field-emission gun–SEM (FEG–SEM), in backscattered electron (BSE) mode, with an accelerating voltage of 20 kV. TEM was carried out using a JEOL JEM F200 TEM in bright-field and dark-field mode, with a voltage of 200 kV. Diffraction patterns were acquired in TEM mode via selected-area diffraction (SADP).

All Vickers hardness testing (unless stated otherwise) was conducted using a standard Vickers indenter (macrohardness), with a load of 30 kgf. Each hardness measurement was repeated for a minimum of five indents distributed across the sample surface. Macrohardness was chosen to allow a bulk hardness value for various samples to be compared. All tensile and Charpy testing was carried out at room temperature by Element and Special Testing Ltd, respectively, both UKAS/NADCAP approved test houses.

The β-approach curve for the new alloy was determined experimentally by heat treating 20 × 10 × 10 mm cubes to various temperatures before immediately water quenching to retain the high-temperature microstructure. Samples were coated in a Prince Lubricants glass lubricant, often used in closed-die forging of titanium, to limit oxidation. A box furnace with a digital programmable logic controller temperature controller and a secondary type-K thermocouple were used. Following quenching, samples were sectioned in half, mounted, and prepared metallographically. The central region of each sample was analyzed in three locations using SEM. The volume fraction of β-phase present was automatically detected from binarized micrographs using an in-house developed ImageJ[16] script. The values for area fraction of β for each alloy were then plotted against the corresponding heat treatment temperature to give the β-approach curve, allowing the β-transus temperature for the alloy to be approximated.

3. Results and Discussion

3.1. Small-Scale Parametric Study: Microstructural Characterizations

FAST samples were produced with 50%/50% by volume mixed Ti-64/Ti-5553 powders using different processing parameters, to determine the effect on microstructure and hardness properties. A low-magnification cross-polarized light micrograph for each processing condition is shown in **Figure 3**. The dark gray regions are areas of the β-phase of Ti-5553 and the other regions with varying contrast are the dual phase $\alpha + \beta$ microstructure of Ti-64. 975 °C was selected as the lowest processing temperature as it is below the β-transus temperature for Ti-64. At 975 °C, there is a clear distinction between the microstructure of the Ti-64 and Ti-5553 regions, with little change visible as the dwell time is increased from 10 to 60 min. The microstructure of the Ti-64 region displays a typical subtransus FAST-processed near-equiaxed microstructure.

At 1000 °C, the 10 min dwell time sample shows two distinct microstructural regions of the Ti-64 and Ti-5553, despite being above the β-transus temperature for both Ti-64 (≈995 °C) and Ti-5553 (≈845 °C). This is significant for two reasons: 1) The entire sample transformed to the β-phase, but compositional heterogeneity exists as different regions transformed to β at different temperatures, 2) A greater amount of diffusion occurred as the diffusivity of alloying elements in β titanium is around three times that of α titanium.[17] The Ti-64 microstructure now exemplifies a classic lamellar microstructure, synonymous with cooling from a processing temperature above the β-transus. As the dwell time increases, the distinction between the two alloy regions blurs, with the interface becoming more diffuse due to the greater levels of diffusion occurring at these processing times and temperatures. The prior-β grain size also appears to increase slightly with increased dwell time, in agreement with the observations by Weston et al.[18] This diffuse region separating the regions of the two alloys is the same region observed in the DB in the previous study by Pope et al.[1] with diffusion bonding occurring on a local rather than global scale. A higher-magnification image of the fine microstructure within this diffuse interface region is shown in **Figure 4**.

As the time and temperature increase to the maximum of 1200 °C for 60 min, blurring of the interface continues and is almost indistinguishable after processing at 1200 °C for 30 min. The micrograph at the bottom right of Figure 3, with the maximum time and temperature conditions, has a distinct microstructure compared to either of the parent alloys in the upper left of the figure. Due to the increased energy input into the system (time and temperature), a sufficient level of diffusion has occurred to homogenize the microstructure. The microstructure after these processing conditions shows good homogeneity, with some small regions of the parent alloy microstructures. This could result from insufficient powder mixing or the use of powder with a PSD that is too large for complete homogenization at these processing conditions.

Figure 5 is a high-magnification micrograph of the 50%/50% by volume mixed sample processed at 1200 °C, 60 min. No

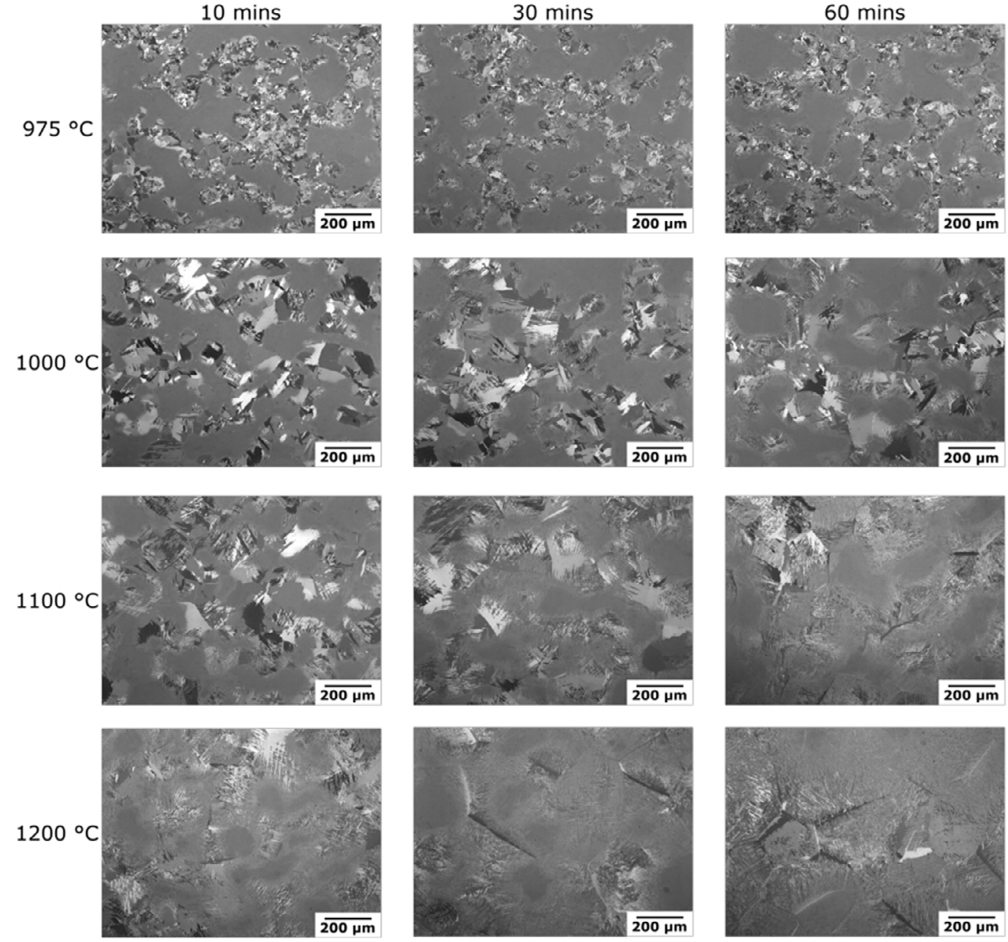

Figure 3. Cross-polarized light micrographs showing the microstructural evolution of 50:50 mixed Ti–64:Ti-5553 sintered samples with increasing dwell time and temperature.

residual regions of the parent alloy microstructures are visible (Figure 5a). On further investigation with SEM (Figure 5b), fine-scale α-laths akin to those previously observed in the DB region were observed. The presence of these fine-scale α-laths indicates that the synergy created previously in the DB can be recreated across small-scale samples and suggests that it is chemistry rather than the DB that forms the microstructure.

Figure 6 shows two TEM images of regions of the sample processed at 1200 °C for 60 min. In both Figure 6, a number of α-laths of various lengths are present within the β-matrix. The width of these laths ranges from 50 to 150 nm, matching that of the fine-scale α, previously observed by Pope et al.[1]

Higher-magnification TEM images are shown in **Figure 7**. The locations labeled 131 and 132 in Figure 7a correspond to the SADPs shown in Figure 7b,c. SADP 131, taken from an α-lath, shows an expected hexagonal pattern, corresponding to the hexagonal close-packed crystal structure of the α phase. SADP 132, taken from a region of the β matrix, shows a rectangular pattern, corresponding to the body-centred cubic crystal structure of the β-phase. The presence of the embrittling and metastable ω phase was hypothesized as a potential reason for the increased hardness of the new alloy; however, neither of the patterns show the characteristic diffuse streaking of diffraction spots commonly associated with the ω phase.[19] Figure 7d shows a Scanning transmission electron micrograph (STEM) image of the central region in Figure 7a. X-ray energy dispersive spectroscopy (X-EDS) data was measured to produce the maps presented in Figure 7e–h that show the distribution of Ti, Al, V, and Mo. The maps show, as expected, that the α-laths are enriched in Ti and Al, with the β-matrix rich in V and Mo.

3.2. Small-Scale Parametric Study: Vickers Hardness Measurements

Vickers hardness (HV30) testing was conducted on each mixed powder sample to enable a comparison between samples and bulk FAST material of each alloy. **Figure 8** shows the measured hardness values which increase as the dwell time and temperature increase. This could be due to increased densification but, there is an increase in hardness of up to ≈18% above monolithic Ti-64 also processed at 1200 °C, 60 min via FAST. Therefore, it is the presence of the fine-scale α regions that have formed between the alloys that is creating a high-hardness material resistant to plastic deformation. This trend of increasing hardness with

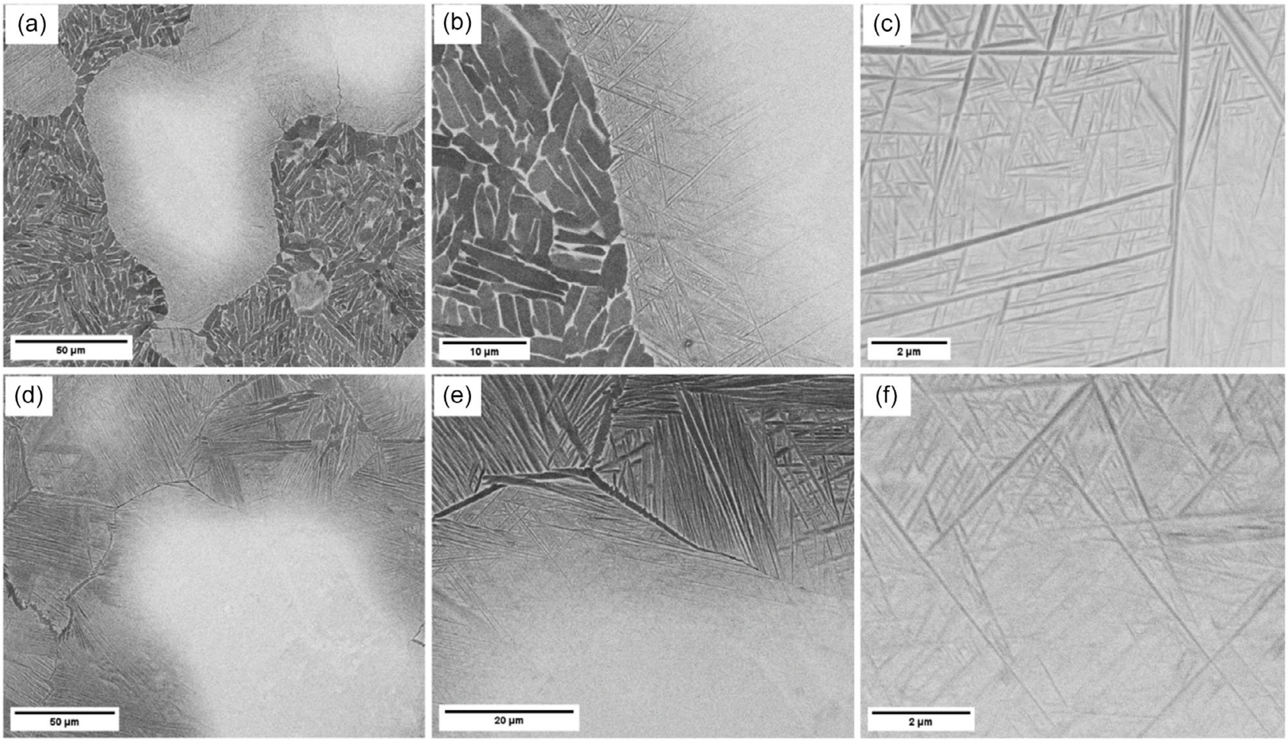

Figure 4. BSE micrographs showing the microstructure of 50:50 mixed Ti-64:Ti-5553 processed via FAST at 975 °C: a–c) and 1000 °C: and d–f) for 60 min.

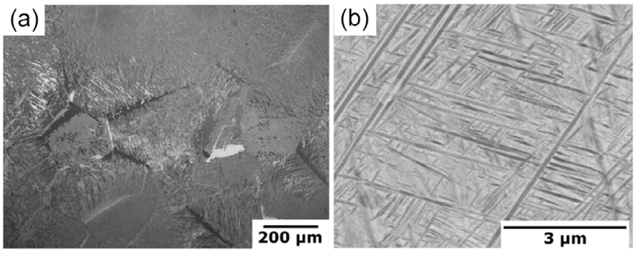

Figure 5. a) Cross-polarized light micrograph showing the microstructure of the 50:50 Ti-64:Ti-5553 sample sintered at 1200 °C for 60 min. b) BSE micrograph showing very fine-scale α-laths present in the microstructure.

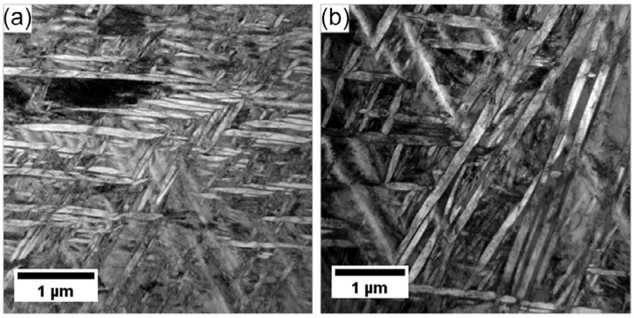

Figure 6. TEM micrographs showing two regions of fine-scale α-precipitates with hierarchical size distributions, with finer laths in a) and slightly coarser laths in b).

processing time and temperature also goes against the trend that would be expected for an increasing prior-β grain size. The peak measured hardness of 395 HV at 1200 °C, 60 min demonstrates the unique synergy created by combining these two alloys.

Some variation is observed in the measured values, shown as error bars in Figure 8, but the variation between samples remains fairly consistent and can be explained by fluctuations in the vol. fraction of fine-scale α per indent and per sample. This is in agreement with the conclusion formed by Lao et al.[20] that variation in secondary α area fraction and spacing causes fluctuations in strength (and hardness).

3.3. Small-Scale Parametric Study: Alternate Mix Ratios

Although 50%:50% by volume was deemed as the optimal mix ratio, small-scale samples were also produced with alternate alloy mix ratios. **Figure 9** shows the hardness variation across different mix ratios of the two parent alloys. The sample consisting of a 50%:50% by volume mix of the two alloys displayed the highest measured hardness value of 389 HV ± 11. The hardnesses at ratios of 40:60 and 60:40 are 386 HV ± 5 and 378 HV ± 21 respectively, indicating that the compositional window of the optimum alloy "sweet spot" is relatively wide. The hardness values decrease as the ratios approach the parent alloy compositions. This figure demonstrates the synergistic effects of combining these two alloys to achieve a compositional "sweet spot" with alloy mixes that have a higher peak in hardness than either of the parent alloys.

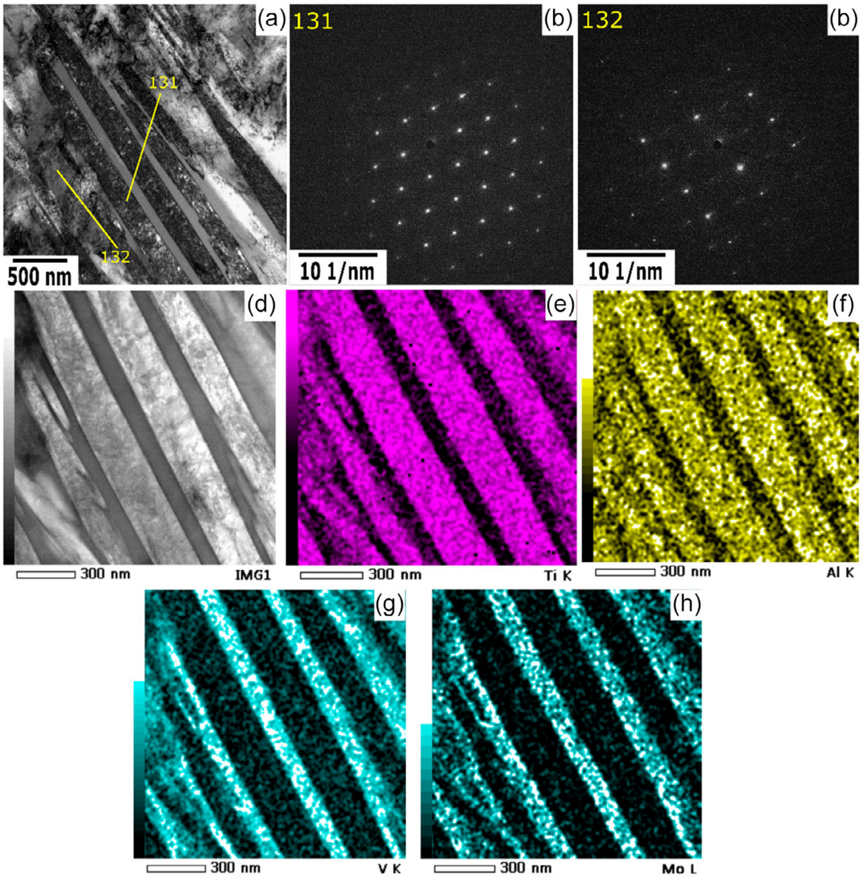

Figure 7. a) TEM micrograph of a region of the microstructure. b) SADP of a region of α-phase. c) SADP of a region of the β-phase. d) STEM micrograph of the same region at slightly higher magnification. e–h) STEM–EDS micrographs for various elements.

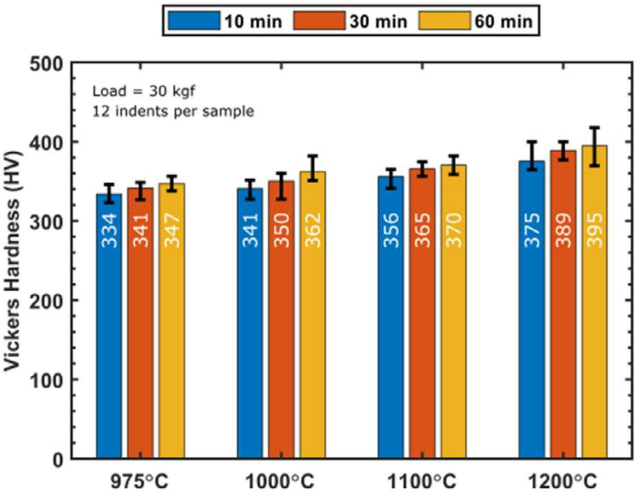

Figure 8. Bar chart showing measured Vickers hardness values for 50:50 mixed Ti-64:Ti-5553 sintered samples. (Note: Error bars show range of max to min values measured).

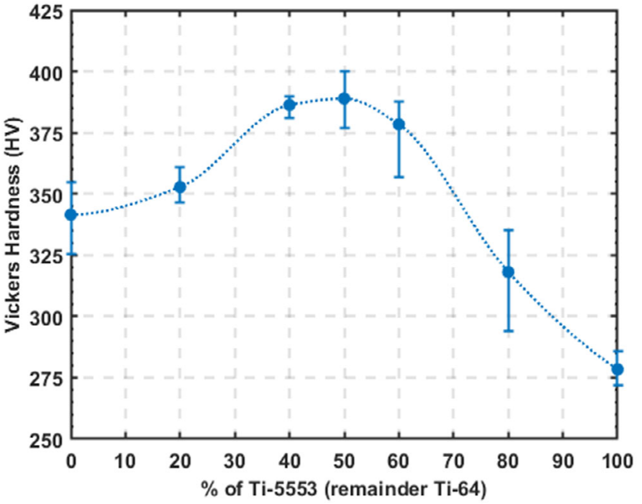

Figure 9. Scatter plot showing the measured Vickers hardness values for various alloy mix ratios when processed at 1200 °C, 60 min via FAST. (Note: blue dashed line is a visual guide to the eye rather than a trendline and error bars show the range of max to min values measured).

3.4. Small-Scale Parametric Study: β-Approach Curve

Figure 10 shows the measured β-approach curve for the new alloy. Samples were analyzed after heating to six temperatures: 860, 880, 900, 910, 930, and 950 °C. The microstructure in samples heated to 860 and 910 °C evolves from a Widmanstätten-like structure made up of acicular α laths at 860 °C to having much more isolated α plates surrounded by β-matrix at 910 °C.

From the data in Figure 10, the transus temperature for the new alloy lies between 935 and 950 °C. While this experiment gave a good indication of the transus temperature and approach curve, there is a large amount of uncertainty due to the mixing of the two alloys together to achieve the new alloy. Microstructural observations have shown that chemical heterogeneities remain after FAST processing and after these heat treatments. During the analysis of the microstructure of the heat-treated samples, it was clear that some regions of the microstructure had a different transus temperature to others, dependent on the chemistry in that region. Further analysis of a cast + wrought version of the same novel alloy composition, from currently unpublished work, provides confidence that the β-transus temperature is around 935 °C. As expected, the transus temperature for the new alloy falls somewhere in between those of the two parent alloys. When comparing the gradient of the β-approach curve to those recorded in the literature for both Ti-64 and Ti-5553, the curve for the new alloy has a slightly lower gradient than that of Ti-64, suggesting that there is potential for improved hot workability with the new alloy, that is, the α phase volume fraction is less temperature sensitive.

3.5. Large-Scale Mechanical Property Testing

Figure 11 displays the engineering stress–strain curves for all as-FAST samples extracted from Billet 1 (B1) and Billet 2 (B2-A). Despite the differences in cooling rates, the tensile behavior of samples from both billets is very similar, particularly when comparing up to the ultimate tensile strength (UTS). The corresponding average values are given numerically in **Table 3** along with literature values for the parent alloys. The averages demonstrate that the properties are consistent across the two billets, with low standard deviation values, despite the potential for areas of locally different chemistry due to inhomogeneity caused by insufficient mixing of the two powders. This does not inhibit the good tensile performance and may even be beneficial to the plasticity of the alloy as different regions transfer the deformation and load to one another increasing the work hardening of the sample. This observation was previously made by Zafari et al.[7] when combining the same alloys via AM, although the microstructure was very different in that case.

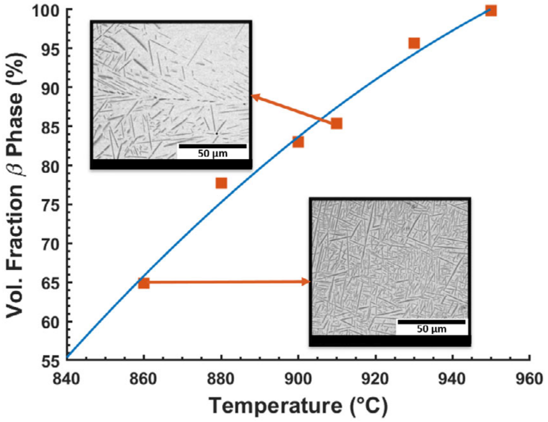

Figure 10. Scatter plot showing the measured β-approach curve for the newly developed alloy, S23, prepared from 50:50 mix of Ti-64:Ti-5553 powders. (Note: blue line is a guide to the eye rather than a trend line).

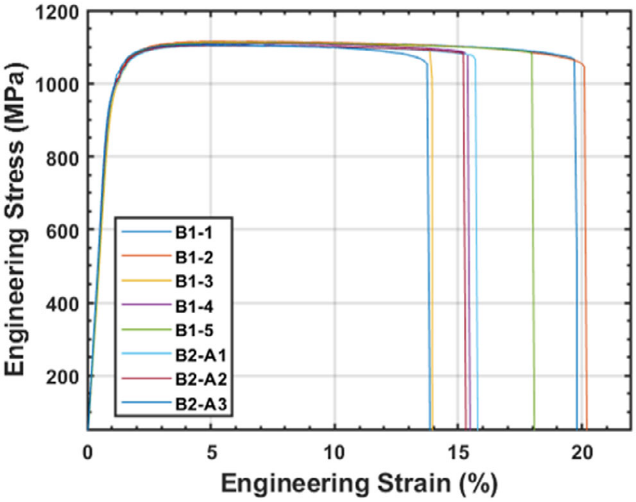

Figure 11. Stress–strain graph showing the tensile curves for eight samples across Billets 1 and 2.

Table 3. A comparison of the recorded YS, UTS, and elongation for the newly developed alloy and literature values for the parent alloys in various conditions.

Material	Condition	0.2% Y.S. [MPa]	UTS [MPa]	Elongation [%]
S23 Billet 1	As-FAST	985 ± 5	1112 ± 8	18 ± 2
S23 Billet 2	As-FAST	980 ± 5	1103 ± 6	15 ± 1
Ti-64[21]	As-FAST (1200 °C, 30 mins)	758	835	8
Ti-5553[21]	As-FAST (1100 °C, 30 mins)	668	747	17
Ti-5553[22]	STA	1170	1240	4
Ti-5553[22]	BASCA	965	1080	6
Ti-64[23]	MA	945	1065	10
Ti-64[23]	DA	917	965	18
Ti-64[23]	STA	1103	1151	13

The tensile properties for the new alloy are promising due to the combination of high strength and excellent ductility (i.e., tensile toughness), when compared with the literature values of the parent alloys (Ti-64 and Ti-5553) in **Figure 12**. A considerable improvement over the monolithic alloys produced with FAST is also clear, demonstrating the synergy created by combining

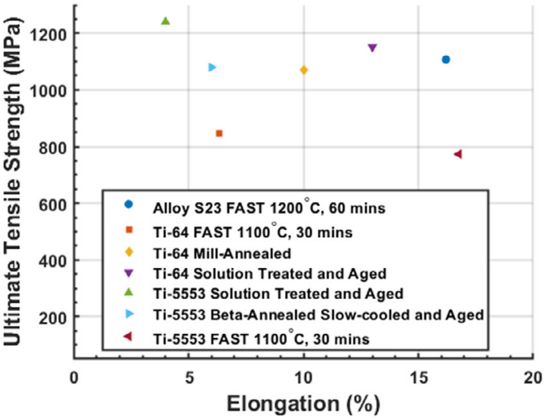

Figure 12. Scatter plot showing the UTS versus elongation for the new alloy (S23), compared to the parent alloys in the as-FAST condition and literature values (referenced in the table above).

the two alloys, despite this system being highly unoptimized. Additionally, the material described in the literature is produced via a conventional melt-wrought route, compared to the FAST material which has been consolidated from powder, in as little as one hour processing time.

Charpy impact (V-notch) testing of the new alloy gave a value of 21 ± 2 J, further demonstrating that the newly developed alloy exhibits at least comparable properties to Ti-64, with the potential for further enhancements.

These desirable properties provide indications that the combining of surplus commercial powder and scrap material for these two aerospace alloys may be beneficial for sustainability and performance. There is also potential for further improvements with optimized processing parameters, improved homogeneity, conventional cast + wrought processing, heat treatment, and subsequent thermomechanical processing. For example, producing a prealloyed S23 powder of the novel composition would allow the FAST processing parameters to be optimized and enable the processing of a more equiaxed or bimodal microstructure which would be beneficial for fatigue properties.

4. Conclusion

This article presents a new alloy, termed S23, derived from a compositional "sweet spot" between two commercially available aerospace titanium alloys: Ti-64 and Ti-5553. Surplus powders of the two alloys were combined and processed via FAST and a high-strength, high-ductility new β-rich $\alpha + \beta$ alloy was created with the composition: Ti–5.5Al–4.5V–2.5Mo–1.5Cr. Tensile results show exceptional tensile toughness when compared with the parent alloys in a range of conditions. In-depth microstructural analysis reveals the presence of fine-scale α precipitates, which form despite the relatively slow cooling rates experienced, providing the excellent balance of properties. Further work is ongoing by the UK aerospace industry to determine the hot forging behavior and fatigue properties of the new alloy in both powder and cast-wrought forms.

Acknowledgements

S.L. was funded by Science Foundation Ireland (18/EPSRC-CDT/3584) and the Engineering and Physical Sciences Research Council UK (EP/S022635/1) through the Advanced Metallic Systems Centre for Doctoral Training. The authors acknowledge financial support from the UKRI-EPSRC MAPP Future Manufacturing Hub (EP/P006566/1, www.mapp.ac.UK). S.L. also acknowledges the financial support of the project by Rolls-Royce plc. The authors would like to thank Dr. John Nutter for assistance with transmission electron microscopy and Dr. Oliver Levano Blanch for useful discussions.

Conflict of Interest

The authors declare no conflict of interest.

Author Contributions

Samuel Lister: formal analysis (lead); investigation (lead); methodology (lead); validation (lead); visualization (lead); writing—original draft (lead); writing—review & editing (lead). **Gavin J. Baxter**: conceptualization (equal); methodology (equal); supervision (equal); writing—review & editing (equal). **Martin Jackson**: conceptualization (equal); funding acquisition (lead); project administration (lead); supervision (lead); writing—review & editing (lead).

Data Availability Statement

The data that support the findings of this study are available from the corresponding author upon reasonable request.

Keywords

alloy development, field-assisted sintering technology, recycling, spark plasma sintering, titanium alloys

Received: February 27, 2025
Revised: May 2, 2025

[1] J. J. Pope, E. L. Calvert, N. S. Weston, M. Jackson, *J. Mater. Process. Technol.* **2019**, *269*, 200.
[2] N. S. Weston, M. Jackson, *Metals* **2020**, *10*, 296.
[3] S. Lister, O. Levano Blanch, D. Suarez Fernandez, J. Pope, G. J. Baxter, S. Bray, *Metall. Mater. Trans. A Phys. Metall. Mater. Sci.* **2023**, *54*, 4396.
[4] A. E. Davis, C. I. Breheny, J. Fellowes, U. Nwankpa, F. Martina, J. Ding, T. Machry, P. B. Prangnell *Mater Sci Eng A.* **2019**, *765*, 138289.
[5] J. R. Kennedy, A. E. Davis, A. E. Caballero, M. White, J. Fellowes, E. J. Pickering, P. B. Prangnell, *Mater. Charact.* **2021**, *182*, 111577.
[6] A. Zafari, K. Xia, *Mater. Res. Lett.* **2018**, *6*, 627.
[7] A. Zafari, K. Xia, *Scr. Mater.* **2019**, *173*, 61.
[8] S. A. Mantri, D. Choudhuri, A. Behera, J. D. Cotton, N. Kumar, R. Banerjee, *Metall. Mater. Trans. A Phys. Metall. Mater. Sci.* **2015**, *46*, 2803.
[9] A. Devaraj, V. V. Joshi, A. Srivastava, S. Manandhar, V. Moxson, V. A. Duz, C. Lavender, *Nat. Commun.* **2016**, *7*, 1.
[10] Y. Zheng, R. E. A. Williams, D. Wang, R. Shi, S. Nag, P. Kami, J. M. Sosa, R. Banerjee, Y. Wang, H. L. Fraser, *Acta Mater.* **2016**, *103*, 850.

[11] J. Coakley, V. A. Vorontsov, N. G. Jones, A. Radecka, P. A. J. Bagot, K. C. Littrell, R. K. Heenan, F. Hu, A. P. Magyar, D. C. Bell, D. Dye, *J. Alloys Compd.* **2015**, *646*, 946.

[12] Y. Jia, H. Su, S. Cao, R. Shi, Y. Ma, Q. Wang, S. Huang, R. Zhang, Q. Hu, Y. Zheng, S. Zheng, J. Lei, R. Yang, *Acta Mater.*, **2024**, *279*, 120302.

[13] M. Wang, Y. Lu, B. Pang, Z. T. Kloenne, H. L. Fraser, Y. L. Chiu, M. H. Loretto, *Acta Mater.* **2019**, *173*, 242.

[14] A. Devaraj, S. Nag, R. Banerjee, *Scr. Mater.* **2013**, *69*, 513.

[15] S. Nag, Y. Zheng, R. E. A. Williams, A. Devaraj, A. Boyne, Y. Wang, P. C. Collins, G. B. Viswanathan, J. S. Tiley, B. C. Muddle, R. Banerjee, H. L. Fraser, *Acta Mater.* **2012**, *60*, 6247.

[16] R. Bourne, *Fundam. Digit. Imaging Med.* **2010**, *9*, 185.

[17] G. Lütjering, J. C. Williams, *Titanium*, 2nd ed., Springer, Berlin **2007**.

[18] N. S. Weston, F. Derguti, A. Tudball, M. Jackson, *J. Mater. Sci.* **2015**, *50*, 4860.

[19] D. De Fontaine, N. E. Paton, J. C. Williams, *Acta Metall.* **1971**, *19*, 1153.

[20] Z. Lao, H. Zhang, S. Wang, G. Zhou, S. Zhang, L. Chen, Q. Li, *J. Mater. Eng. Perform.* **2025**, *34*, 6553.

[21] T. Virazels, S. Lister, O. Levano-Blanch, M. Jackson, J. Rodríguez-Martínez, J. Nieto-Fuentes, *Int. J. Fract.* **2025**, *123*, 183.

[22] J. D. Cotton, R. D. Briggs, R. R. Boyer, S. Tamirisakandala, P. Russo, N. Shchetnikov, J. C. Fanning, *JOM* **2015**, *67*, 1281.

[23] M. J. Donachie, *Titanium - A Technical Guide*, 2nd ed., Vol. *99*, ASM International, Materials Park, OH **2000**.